Research of Pattern Formation, edited by R. Takaki, pp. 131–154.

Monte Carlo Simulation and Single Nucleation Theory of Growth Shapes of a Crystal

Tsuyoshi UETA and Yukio SAITO

Department of Physics, Keio University,
3-14-1 Hiyoshi, Kohoku-ku, Yokohama 223, Japan

Abstract. Crystal growth in a diffusion field is studied by means of a lattice gas model. In a closed system the crystal takes an equilibrium form, whereas in an open system where the crystal is in contact with a gas reservoir , the crystal grows steadily. For a small crystal or at a small chemical potential difference $\Delta\mu$ between the gas and the crystal, the growth form is polygonal. On increasing $\Delta\mu$ or for a large crystal, it varies to hopper-like, to dendritic and finally to a fractal structure. The variations of the growth shape as a function of the temperature and of the gas density are also investigated. The growth rate and the size of a polygonal crystal are interpreted by a single nucleation and growth mechanism.

1. Introduction

Recently intensive studies have been done on pattern formations as it is a typical problem of nonequilibrium statistical physics. Crystal growth is one of these pattern formation phenomenon (1). Crystal has shown various beautiful and mysterious forms. Morphology of a crystal reflects its history during the growth and includes various interesting physical phenomena. Therefore, it has been investigated for a long time, while our understanding of its form is still immature. The main cause of this unsatisfactory situation is that the crystal growth or the pattern formation is a dynamical and nonlinear phenomena, and the well founded methods of equilibrium statistical mechanics and linear analysis are not applicable. Our main concern

here is the understanding of the morphology of a crystal growing in a mass or a heat diffusion field. The growth form depends on a surface tension and on a surface kinetics. If the solidification is controlled by the surface kinetics with singularity, the crystal is enclosed by faceted faces (2). If a local equilibrium on a crystal surface holds, its shape is governed by an interfacial tension and turns into a dendritic form with a parabolic tip and almost regular sidebranches (1, 3, 4). In the limit of vanishing interfacial energy, patterns become fractal, whose structure is characterized by a fractal dimension D_f (5).

In macroscopic theories of the solidification (1, 7, 8, 9, 10, 11), and related phenomena, the surface tension and kinetics are treated phenomenologically and are given as an input parameter. On the other hand, in the theories of equilibrium phase transitions of an interface as a roughening or a faceting transition (12, 13, 14) the surface tension is treated microscopically. In this paper we propose a simple microscopic model of a crystal growing in a diffusion field, such that the equilibrium and the growth forms of the crystal are treated in a unified way (15). By means of extensive Monte Carlo simulations, equilibrium and growth forms are obtained under various conditions of the temperature, chemical potential and the gas density. The growth velocity and the maximum size of a polygonal crystal are explained in terms of a stable single nucleation theory.

2. The Model and the Simulation Algorithm

In order to treat microscopically a situation where a solid coexists with a gas, we introduce a simple model in which the gas and the solid phases consist of their respective atoms. A gas atom is mobile to give an entropy contribution to the chemical potential, whereas a solid atom is immobile but its chemical potential has a contribution from the energy.

The situation is further simplified by considering a lattice system, where the space is divided into discrete lattice points. Each lattice site can be occupied by a solid atom, by a gas atom or can be empty. Double occupancy of a lattice site is forbidden. The crystal we consider lies on a square lattice. Since the system has four-fold symmetry, we consider only an upper-right quarter of a crystal nucleus in the positive x and y region. In order to fix the center of the mass at the origin, a skewed boundary condition is assumed so that the x- and y-axes are contiguous to each other.

The attractive interaction is assumed between the nearest neighboring solid atoms. Gas atoms are assumed to have no interaction so as to suppress the polynucleation process. When a solid atom evaporates, it costs an energy μ_c (>0), whereas a gas atom gains entropy by exchanging its position with a neighboring empty site. This exchange process mimics the diffusion in a gas phase. These energetics are summerized in a Hamiltonian

$$H = -\varepsilon \sum_{\langle i\ j \rangle} n_i n_j - \mu_c \sum_i n_i \tag{1}$$

where the first summation runs over all the nearest neighbor pairs, and the crystallization order parameter n_i on an i-th lattice site is unity when it is occupied by a solid atom and vanishes otherwise. In terms of an Ising spin variable, $S_i \equiv 2n_i - 1 = \pm 1$, the Hamiltonian reduces to that of a ferromagnetic Ising model in a field;

$$H = -J \sum_{\langle i\ j \rangle} S_i S_j - \frac{\mu_s}{2} \sum_i S_i + \text{const} \tag{2}$$

with $J = \varepsilon/4$, $\mu_s = \mu_c + z\varepsilon/2$ and z being the coordination number.

We perform Monte Carlo simulations of the lattice gas model, Eq. (1), to obtain crystal shapes. Stochastic evolution of the system consists of the following steps: Every gas atom hops freely from a lattice site to one of its nearest neighbors, unless it is occupied. When a gas atom diffuses to come into contact with solid atoms, it crystallizes with a probability W. Inverse to this crystallization process is an evaporation, where a solid atom at an interface tries to turn into a gas atom. These crystallization and evaporation processes at the interface should satisfy the detailed balance condition. We have adapted the heatbath algorithm: Transition probability W for a process with an energy change ΔE at a temperature T is set to be $W(\Delta E) = [1 + \exp(\Delta E/T)]^{-1}$. We neglect evaporation in the bulk crystal and solidification in the bulk of the gas phase, since our main concern is on the crystal morphology at low temperatures where these excitations in bulk phases are quite rare.

A simulation starts with a solid nucleus situated in a closed vessel. Some solid atoms evaporate to a gas phase and diffuse away from the interface, but some gas atoms condense back. From this simulation, we get an equilibrium form of the crystal (12, 13, 14). Instead, if the system is expanded steadily by providing an atom reservoir with a prescribed gas density at the periphery of the system, crystal continues to grow and we get a growth form.

3. Equilibrium Shape and Size

Wulff's theorem states that an equilibrium shape of a crystal can be constructed from an orientation-dependent surface tension $\gamma(\theta)$ (16). Since our model, Eq. (1), corresponds to the Ising ferromagnet, Eq. (2), $\gamma(\theta)$ is exactly known for a square lattice (14). The theoretical profile is compared with the simulated shape to test our simulation algorithm.

In Fig. 1 we show an averaged interface profile at temperatures a) $T/J = 0.3$ and b) $T/J = 0.6$ (15). These temperatures are far below the Ising critical temperature $T_c/J = 2/\ln(1 + \sqrt{2}) \approx 2.27$ and assures the absence of a hole creation in the crystal

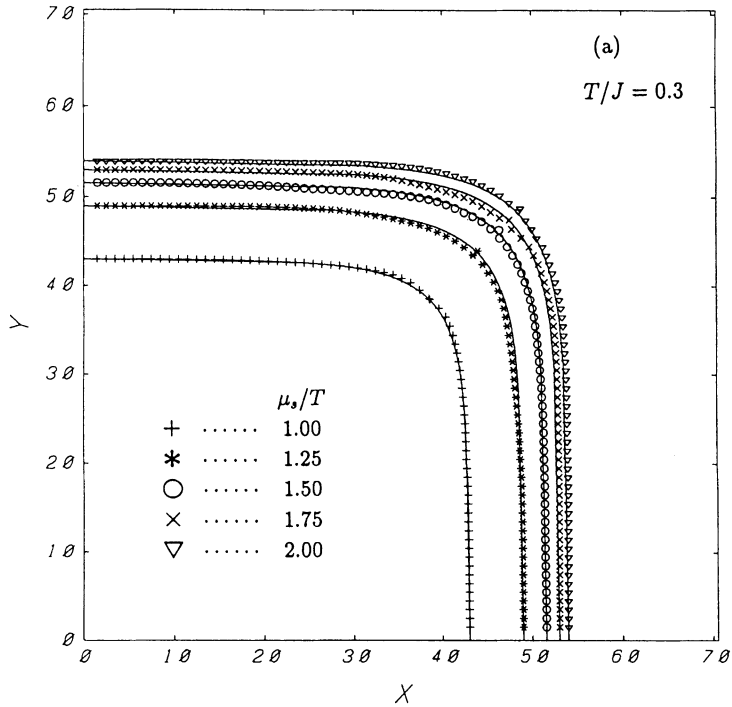

Fig. 1

nucleus. At each temperature crystal shapes for various chemical potentials μ_s are similar, but the size increases as μ_s increases. On heating the system the crystal shape becomes rounded.

Our simulation profiles agree with theoretical ones which are drawn by curves in Fig. 1 with an adjustment in the top height of the crystal. The size of a nucleus, N_s, obtained by the simulation agrees with the expectation calculated from the free energy minimization; (15)

$$N_s = \left(\frac{\bar{\gamma}(T)}{\Delta\mu} \right)^2 \tag{3}$$

where $\Delta\mu = \mu_s - \mu_g$ is the chemical potential difference between the solid μ_s and the gas, $\mu_g = -T\ln(n_g)$ of density n_g and $\bar{\gamma}(T)$ is the averaged surface tension.

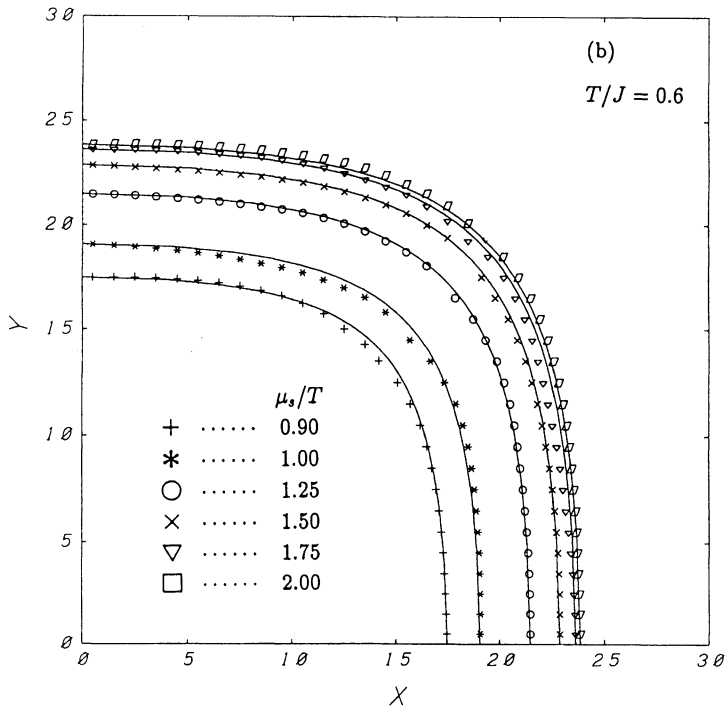

Fig. 1. Average interfacial profiles at (a) $T/J = 0.3$ and (b) $T/J = 0.6$ with various chemical potentials. Curves are the exact profile of the two-dimensional Ising model. The top height is fitted to the simulated profile.

4. Growth Shape

4.1 Simulation of an open system

In an open system where the volume is expanding, the crystal grows. In order to measure a time, we introduce a time unit such that a single diffusion trial of a gas atom corresponds to a time increment of $\Delta t = (4N_g)^{-1}$ when there are N_g gas atoms. By choosing the lattice parameter as a unit of length, the diffusion constant D then reduces to unity. We prepare a list of gas and the interfacial solid atoms, and select an atom from the list randomly. If it is a gas atom diffusion is tried, and when its new position is next to the solid atom solidification is tried. If the selected is a solid atom, evaporation is tried. Therefore, in a time increment of $\Delta t = 1/4$ each gas atom tries diffusion as well as solidification if possible, and each solid atom on the interface tries evaporation once on the average. The vessel is assumed to have a circular shape in order to lessen an anisotropy in the diffusion field.

Simulations are performed at low temperatures as $T/J = 0.3 \sim 1.2$. A chemical

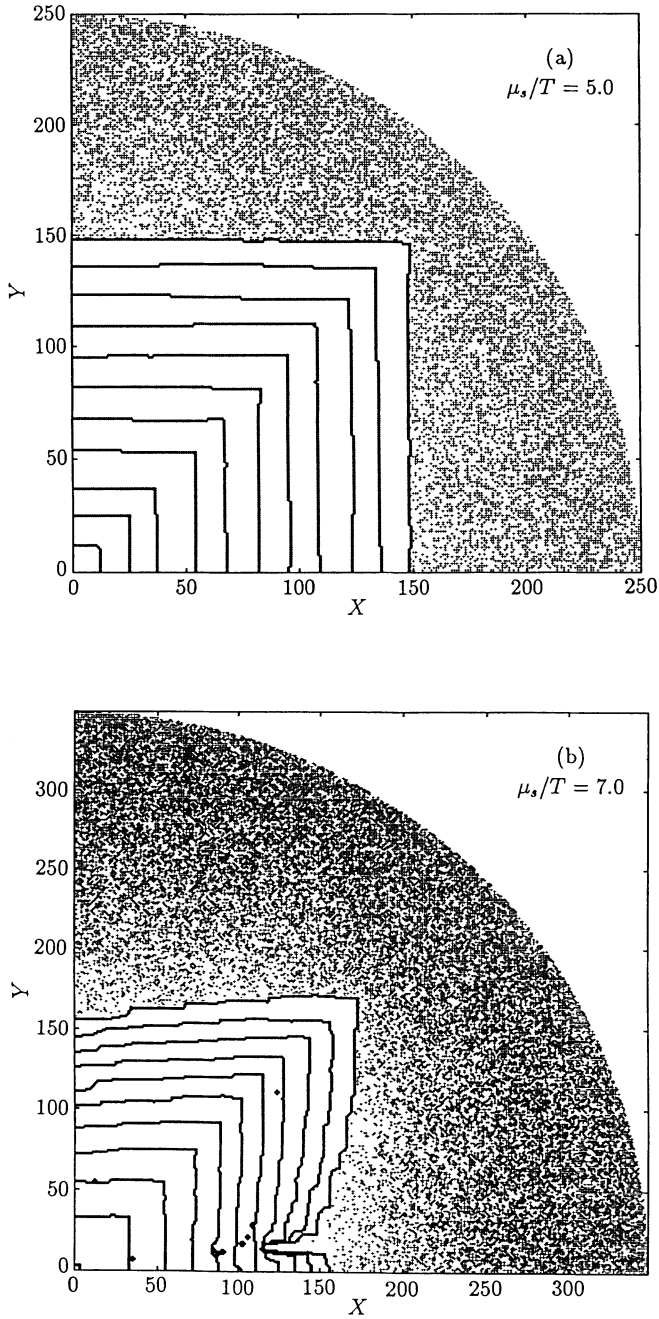

Fig. 2

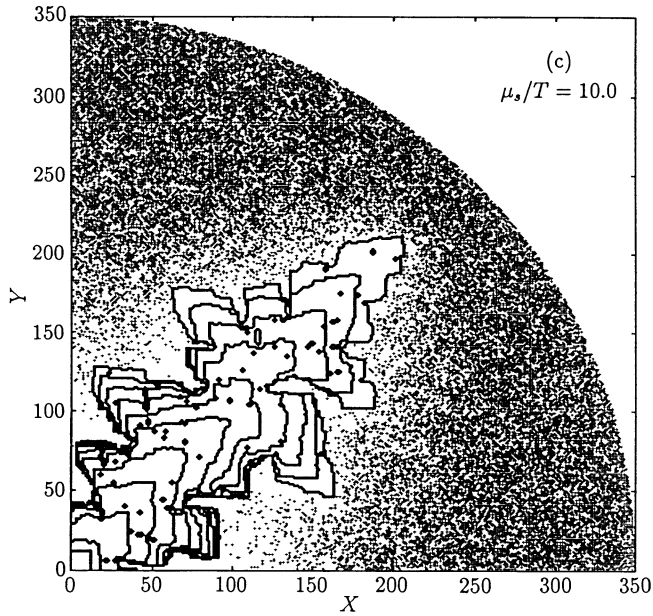
(c)
$\mu_s/T = 10.0$
Y
X
0
50
100
150
200
250
300
350

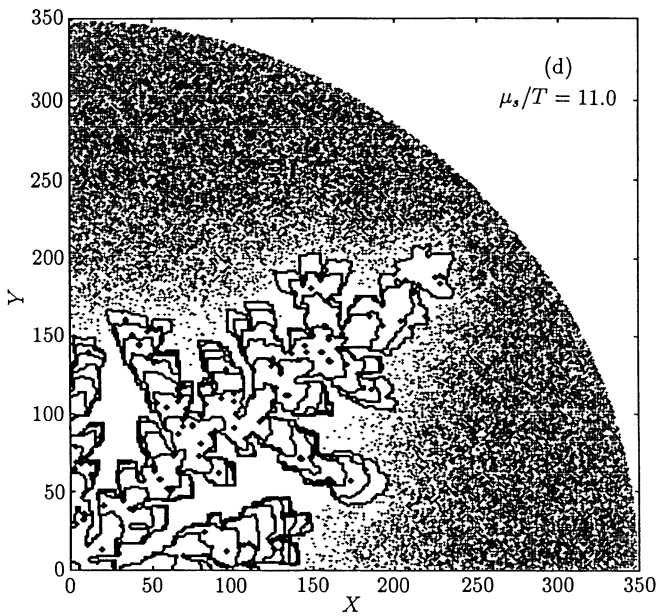
(d)
$\mu_s/T = 11.0$
Y
X
0
50
100
150
200
250
300
350

Fig. 2

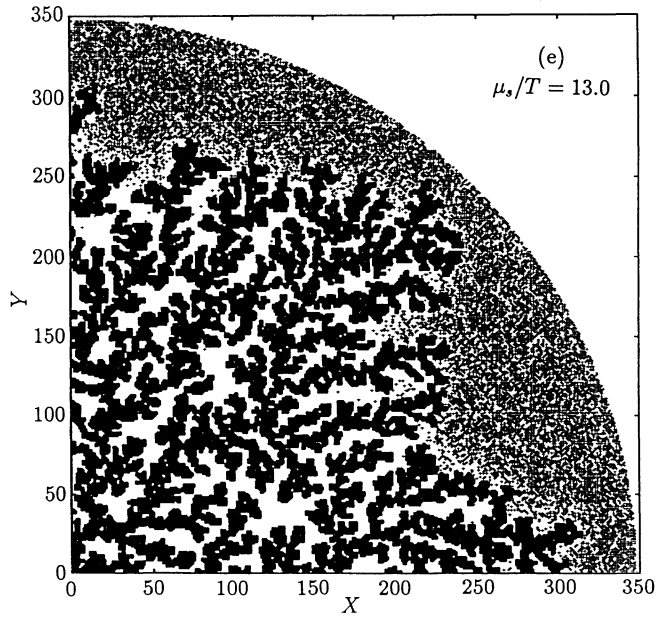

Fig. 2. Stroboscopic growth shapes of the crystal at various μ_s for $T/J = 0.3$ and $n_g = 0.5$. Gas atoms are distributed around the final configurations of the crystal. Chemical potential μ_s/T is (a) 5.0, (b) 7.0, (c) 10.0, (d) 11.0 and (e) 13.0. For (e) only the final crystal shape is shown in black.

potential μ_s is chosen such that the gas density n_g is higher than the thermodynamic equilibrium density $n_{g,eq} = \exp(-\mu_s/T)$. The crystal is then surrounded by a supersaturated gas. By setting an initial size of a crystal nucleus larger than the critical one Eq. (3), the crystal starts to grow.

For a continuous growth of the crystal, we provide a particle reservoir at the periphery of the vessel, which is a thin region of a fixed gas-density. The reservoir should be set far enough from the interface in order not to disturb the gas density distribution. When the crystal grows, it absorbs surrounding gas atoms and the density around the crystal is suppressed. The natural length scale which characterizes the variation of the diffusion field is the diffusion length $l = 2D/V$ for a crystal growing with a velocity V. The best way to shift the particle reservoir outward is, therefore, to keep its separation from the crystal tip longer than l. This scheme is applicable at high μ_s/T. We call this boundary condition as **B.C.1**. At small μ_s, however, the crystal grows very slowly, and the diffusion length $l = 2D/V$ is very long. In order to keep the system small enough and realize simulation, we choose another boundary condition: The particle reservoir is shifted outwardly when the density in front of this region is depressed lower than the level of random fluctuation from the prescribed value, namely below 96% of n_g. We call such a boundary condition

B.C.2. At $\mu_s/T = 8.0$ simulations with two different boundary conditions, **B.C.1** and **B.C.2**, yield similar shape evolution, and the velocities agree with each other.

4.2 Structure

We describe simulation results at a temperature $T/J = 0.3$. Growth shapes vary on increasing the energy gain μ_s/T, as is shown in Fig. 2. At small $\mu_s/T = 4.0$ and 5.0 crystal grows slowly and its shape is polygonal up to our maximum simulation size (Fig. 2a). On increasing μ_s/T from 6.0 to 10.0, the crystal grows initially in a square form, but becomes unstable at the corner, and turns into a dendritic form ultimately (Figs. 2b, c). Further increase in μ_s/T leads to the splitting of the dendritic tip and many irregular branches are observed (Fig. 2d). Until $\mu_s/T = 12$ the structure is rather open, but for $\mu_s/T \geq \mu_{s,th}/T = 13$ the width and the spacing between dendritic branches becomes very fine and the whole structure looks homogeneous (Fig. 2e). This structural change around $\mu_{s,th}$ is caused by the variation in the growth mechanism, and will be discussed in relation to the growth rate.

4.3 Growth rate

The dynamics of the crystal growth is resolved from the time evolution of the crystal tip. A separation r_{tip} of the farthest tip of the crystal from the origin increases asymptotically in proportion to the time t. Growth rate is defined by the time variation of r_{tip} as $V = \Delta r_{tip}/\Delta t$. When the crystal grows in a square form or in an open dendritic form, the growth rate is very small (Fig. 3a). In the previous paper (15), by fitting V for $11 \geq \mu_s/T \geq 4$ we obtained the relation

$$V \sim \exp\left(-0.29(\varepsilon - \mu_s)/T\right) \tag{4}$$

On the other hand, for μ_s/T higher than $\mu_{s,th}/T \sim 13 \sim \varepsilon/T\ (= 4J/T)$, the energy barrier against nucleation, $\varepsilon - \mu_s$, vanishes and most gas atoms solidify when they attach to the crystal surface. The velocity V at large μ_s's increases drastically compared to the nucleation growth rate at small μ_s's. The diffusion length is here less than unity.

When μ_s is infinite, a gas atom solidifies instantaneously as it touches the solid aggregate. The problem is the same with the DLA model growing in a gas of a finite density. In fact, the rate $V(\mu_s = \infty) = 3.25$ (15) is a little smaller but of the same order of the value $V = 3.64$ obtained in the DLA growth simulation from a linear seed of the solid (17).

4.4 The stability limit of a square crystal

To represent the structure of an aggregate, the fractal dimension D_f defined by $N_s \sim R_g^{Df}$ is often used, where $R_g = \left(1/N_s \sum_{i=1}^{N_s} r_i^2\right)^{1/2}$ being the radius of gyration. We have estimated the exponent D_f at various μ_s's for the dendritic growth and

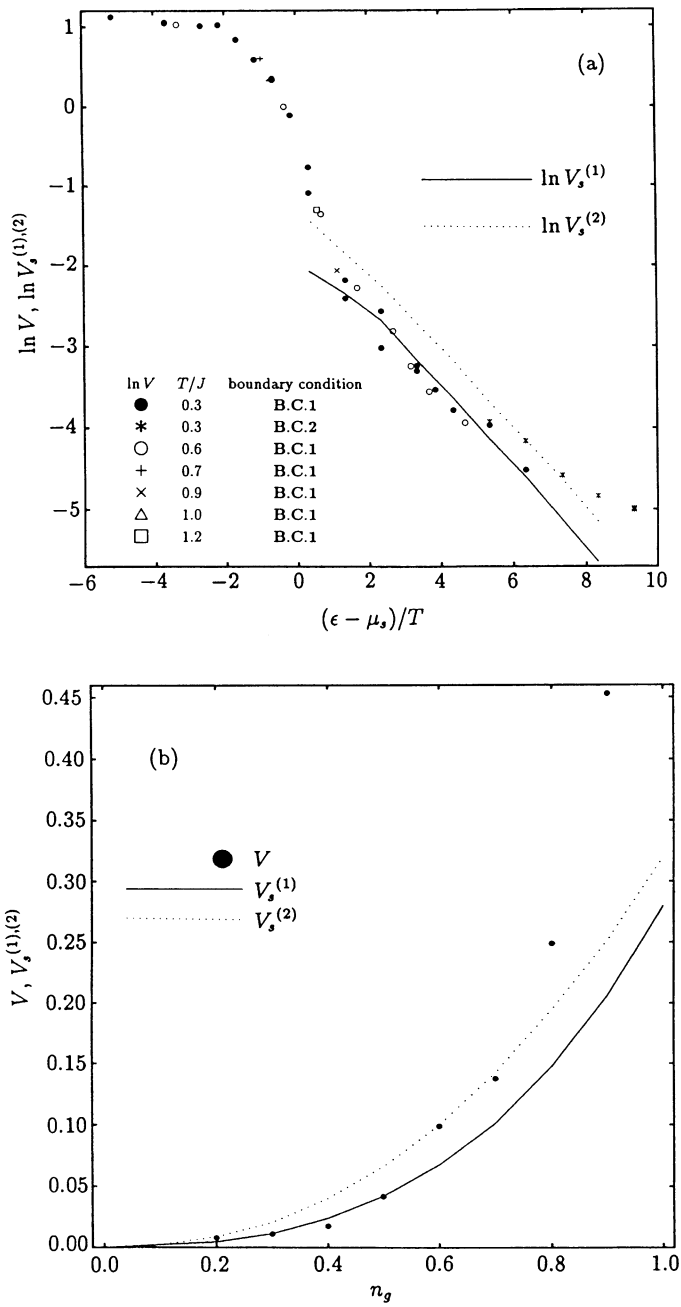

Fig. 3. (a) The $(\varepsilon - \mu_s)/T$-dependence of ln V and ln $V_s^{(1),(2)}$ at $n_g = 0.5$, $T/J = 0.3$. (b) The n_g-dependence of V and $V_s^{(1),(2)}$ at $\mu_s/T = 10.0$ and $T/J = 0.3$.

obtained the value around 1.7 (15), quite similar to the fractal dimension of the DLA (5), but the dendrite here is almost regular. The value of D_f smaller than the space dimension $d=2$ does not necessarily mean the irregular fractal structure but merely represents the openness of the structure.

For μ_s higher than $\mu_{s,th}$ the diffusion length is less than unity, and the growth form shows very fine structure. The exponent D_f of the aggregate agrees now to the space dimension $d=2$ indicating that the system is homogeneous (17). Even though D_f is equal to $d=2$ both at very small and large μ_s's, the crystal structure is quite different: a polygonal structure at small μ_s's and an irregular compact structure at large μ_s's. The difference can not be represented by means of the fractal dimension.

The difference becomes obvious in looking at the number of the interfacial solid atoms $N_{s,i}$. When a crystal grows in a square form to a size N_s, $N_{s,i}$ is expected to be proportional to the linear dimension or the peripheral length $2\sqrt{N_s}-1$, whereas for a ramified compact structure, $N_{s,i}$ is expected to be proportional to N_s. Therefore, we define a parameter $S(t)$ by

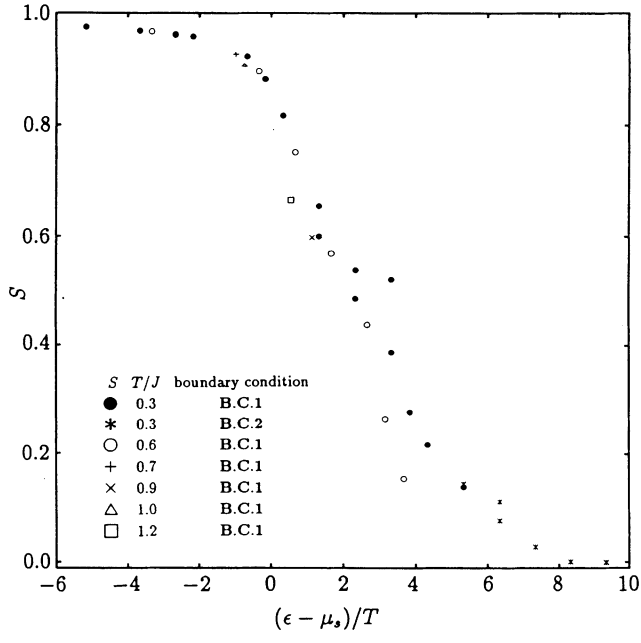

Fig. 4. Structure indicator S, which relates the number of interfacial solid atoms $N_{s,i}$ to that of the total solid atoms N_s, plotted vs $(\varepsilon-\mu_s)/T$ with $n_g=0.5$.

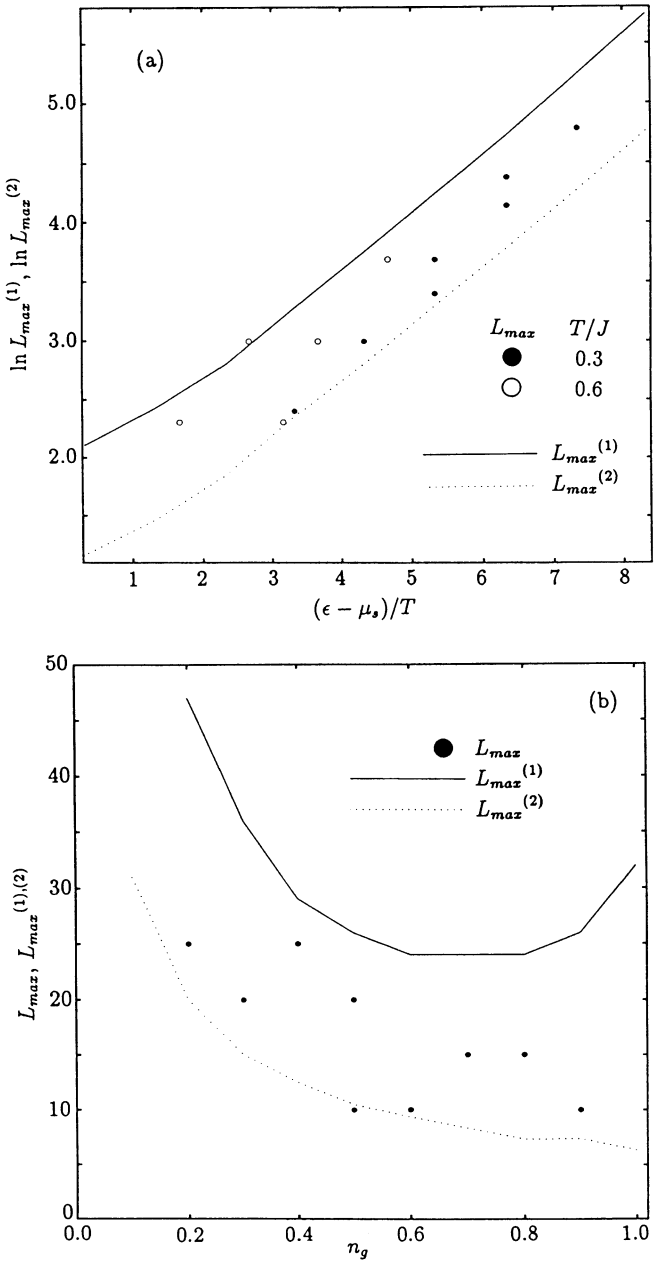

Fig. 5. (a) The $(\varepsilon - \mu_s)/T$-dependence of the stability limit L_{max} by the Monte Carlo simulation and $L_{max}^{(1),(2)}$ at $n_g = 0.5$, $T/J = 0.3$. (b) The n_g-dependence of the stability limit L_{max} and $L_{max}^{(1),(2)}$ at $\mu_s/T = 10.0$, $T/J = 0.3$.

$$S = \frac{\ln\left(N_{s,i} / \left(2\sqrt{N_s - 1}\right)\right)}{\ln\left(N_s / \left(2\sqrt{N_s - 1}\right)\right)}. \tag{5}$$

Figure 4 depicts the variation of the parameter S as a function of the solid chemical potential $(\varepsilon - \mu_s)/T$. At a small μ_s and for small crystals, S vanishes, representing that the shape is polygonal. At large μ_s or for a large crystal, S becomes of order unity, representing that the shape is complicated and a finite fraction of solid atoms are located on the interface.

At intermediate values of μ_s, crystal morphology changes, as the crystal grows, from a small polygonal shape to a large dendritic one. In order to characterize this morphological change at a fixed μ_s, we estimate the stability limit of the square crystal, L_{max}, such that for $L(t) \equiv \sqrt{N_s(t)} < L_{max}$, $S(t)$ is about 0, while for $L(t) > L_{max}$, $S(t)$ deviates significantly from zero. It is observed that L_{max} depends exponentially on the chemical potential μ_s (Fig. 5a). The least-squres fit leads to the relation (15);

$$L_{max} \sim \exp\left(0.59\left(\varepsilon - \mu_s\right) / T\right) \tag{6}$$

When the crystal grows larger than L_{max}, it takes a dendritic profile, but the tip size and the sidebranch periodicity of the dendritic structure still seem to be scaled with L_{max}, as shown in Fig. 2. Thus, L_{max} characterizes the structure in the crystal. Discussion on the L_{max} will be given later in terms of the nucleation theory.

4.5 Temperature and the gas density variation

We perform simulations at a higher temperature $T/J = 0.6$ with various μ_s. Variations in structures and in growth rate as a function of μ_s's are quite similar to those at a temperature $T/J = 0.3$ except the threshold value of $\mu_{s,th}$. Now, $\mu_{s,th}/T$ is about 6.67 instead of 13 at $T/J = 0.3$. In both cases, however, $\mu_{s,th}$ itself is about the same as $\varepsilon = 4J$. Therefore, the temperature dependence of the structure and the growth rate is scaled by $(\varepsilon - \mu_s)/T$. The growth rate V and the structure indicator S are plotted against $(\varepsilon - \mu_s)/T$ in Figs. 3a and 4 respectively, in which the results at other temperature are also included. One can note the scaling behavior obviously.

The density dependence of the structure and the growth rate are complex. At a fixed temperature $T/J = 0.3$, simulations for various gas densities were performed at several values of μ_s. We can not find the scaling behavior of the structure indicator S and the growth rate V as a function of $\Delta\mu = \mu_s - \mu_g = \mu_s + T\ln n_g$.

5. Single Nucleation Theory of a Polygonal Crystal Growth

5.1 Diffusion with surface kinetics

In order to understand T-, μ_s- and n_g-dependence of the growth rate and shape of the crystal, we consider the growth of a square-shaped crystal from a diffusion gas field under the control of the surface kinetics. The density of the surrounding gas atoms $C(t, x, y)$ satisfies the diffusion equation

$$\frac{\partial C}{\partial t} = \nabla^2 C(x, y), \tag{7}$$

where the diffusion constant is unity in our unit. The gas density at infinity is kept constant to be n_g. Instead of the Monte Carlo simulation on a discrete lattice gas, we here solve the diffusion equation (7) with boundary conditions determined by the surface kinetics, and study the growth of a square-shaped crystal.

The main contribution to the surface kinetics is the (one-dimensional) nucleation process on a flat edge of the square crystal. An isolated solid atom on the flat edge is unstable due to a large positive energy cost of $\varepsilon - \mu_s$. A stable critical nucleus is a cluster consisting of two neighboring solid atoms. Once a critical nucleus is formed, further spreading costs no energy and a layer growth on the edge takes place quickly. To obtain an explicit expression of the boundary condition for the density field C, we consider a square crystal of a linear dimension $2a$ and surrounded by four lines $x = \pm a$ and $y = \pm a$. In a unit time interval, a flux of an isolated atom, $4C(a, y)P_a$, crystallizes on an edge site (a, y) with $P_a = [1 + \exp((\varepsilon - \mu_s)/T)]^{-1}$. Here the factor 4 comes from our choice of the time unit. This isolated solid atom is easy to be evaporated and has only a very short lifetime:

$$\tau_{ev} = \frac{1}{4}\left[1 + \exp\left(\left(\mu_s - \varepsilon\right) / T\right)\right] \approx \frac{1}{4}.$$

But if one of the neighboring site is crystallized before the isolated atom evaporates, a stable solid nucleus of size two is formed. The conditional probability of the formation of this stable critical nucleus is $\tau_{ev} \cdot 4C(a, y\pm1)P_b$ with $P_b = (1 + \exp(-\mu_s/T))^{-1}$. Due to the thermal fluctuation there is a probability of evaporation to break this nucleus; $\tau_{ev} \cdot 4(1 - P_b)$. The net flux of the formation of a stable nucleus of size 2, which contribute the layer growth, is then obtained as $16C(a, y)\{C(a, y\pm1) - n_{g,eq}\}P_aP_b$, where $n_{g,eq} = P_b/(1 - P_b) = \exp(-\mu_s/T)$ is the equilibrium gas density, already defined. By summing up the whole possible positions of crystallization on the edge, the total probability of forming a minimum stable nucleus is obtained as

$$16P_aP_b\tau_{ev}\left[\sum_{y=1}^{a}C(a\ y)\left\{C(a\ y-1)-n_{g\ eq}\right\}+\sum_{y=0}^{a-1}C(a\ y)\left\{C(a\ y+1)-n_{g\ eq}\right\}\right] \quad (8)$$

The growth rate determined by the surface kinetics is thus approximately written as

$$V_K=32\tau_{ev}P_aP_b\sum_{y=0}^{a-1}\left\{C(a\ y)-n_{g\ eq}\right\}\left\{C(a\ y+1)-n_{g\ eq}\right\} \quad (9)$$

Here we have assumed $n_{g,eq} << C(a, y)$.

In the steady state, gas atoms consumed by the nucleation and growth should be supplied through the diffusion in the bulk of the gas phase. The surface kinetics rate V_K should be balanced with the diffusional rate V_D, as $V_K = V_D = V/\sqrt{2}$, where V is the growth rate in the diagonal direction. The mass deficiency produced per time $\{1 - C(a, y)\}V_D$ should be transported via the diffusional flow, which is proportional to the normal gradient at the interface $\partial C/\partial n$;

$$\left\{1-C(a\ y)\right\}V_D=\frac{\partial C}{\partial x} \quad (10)$$

Since $C(a, y)$ is very small, we may replace the coefficient on the left-hand side to be unity. Thus, on the edge, $x = a(t)$, the conservation equation is written as

$$\frac{da(t)}{dt}=32\tau_{ev}P_aP_b\sum_{y=0}^{a-1}\left\{C(t\ a\ y)-n_{g\ eq}\right\}\left\{C(t\ a\ y+1)-n_{g\ eq}\right\} \quad (11)$$

$$=\left.\frac{\partial C(t\ x\ y)}{\partial x}\right|_{x=a(t)} \quad (12)$$

5.2 Scaling of size and velocity

Before describing the numerical solution of the diffusion equation (7), with boundary conditions Eqs. (11) and (12), we look into the scaling properties of fundamental equations.

The characteristic time and length are the nucleation time

$$\tau_{nuc}=\left[32\tau_{ev}P_aP_b\left(n_g-n_{g\ eq}\right)\right]^{-1} \quad (13)$$

and the corresponding length $l=\sqrt{D\tau_{nuc}}$ with $D=1$. In terms of dimensionless time

and length defined by

$$t = \tau_{nuc} t', \quad \boldsymbol{r} = l\boldsymbol{r}' \quad \text{and} \quad a = la', \tag{14}$$

the dimensionless diffusion field

$$u = \frac{C - n_{g,eq}}{n_g - n_{g,eq}} \tag{15}$$

satisfies the diffusion equation

$$\frac{\partial u(t', x', y')}{\partial t'} = \nabla'^2 u(t', x', y'), \tag{16}$$

with boundary conditions

$$u(R = \infty) = 1 \tag{17}$$

$$\left.\frac{\partial u}{\partial x'}\right|_{x' = a'(t')} = \int_0^{a'(t')} u(t', a'(t'), y') u(t', a'(t'), y' + l^{-1}) dy' \tag{18}$$

$$= \frac{1}{n_g - n_{g,eq}} \frac{da'}{dt'}. \tag{19}$$

In Eq. (18), we transform the summation to an integration. For a slowly growing crystal with $\mu_s << \varepsilon$ or with small l^{-1}, we can neglect the l-dependence of the integrand in Eq. (18). For $\mu_s >> T$, the equilibrium gas density $n_{g,eq}$ is much smaller than n_g and is negligible. Then the dimensionless variables, u and a' depend no more on μ_s or T.

When a crystal grows, it can not keep growing indefinitely in a square form (18). There is a certain limit in a size, $L_{\max}$. The following two criteria are conceivable for the stability limit of the square crystal.

When the gas density on some edge position becomes lower than the equilibrium gas density, a crystal can not maintain a square shape since the evaporation forbids that position to grow. This takes place at the center of the edge where the gas density is minimum among the whole edge sites. Therefore, the first criterion to determine the maximum linear size $L'_{\max}{}^{(1)}$ (in the reduced unit) is

$$\textbf{C1}: \; u\left(L'^{(1)}_{\max}, 0\right) = u\left(0, L'^{(1)}_{\max}\right) = 0. \tag{20}$$

The second criterion represents the effect of kinetic roughening, such that the successive nucleation takes place faster than the completion of a layer growth. Since a crystallization probability per trial at a kink site is $\{C(a, y) - n_{g,eq}\}P_b$, the mean time spent until an atom crystallizes at the kink site is $[4\{C(t, a, j) - n_{g,eq}\}P_b]^{-1}$. Therefore, the spreading time of a single layer after a stable cluster of a size 2 is nucleated at the corner (a, a) is obtained to be

$$\tau_{spr} = \sum_{j=0}^{a-2} \frac{1}{4\{C(t,a,j) - n_{g,eq}\}P_b} \tag{21}$$

If the spreading time, τ_{spr}, is comparable to or longer than the nucleation time,

$$\left[32\,\tau_{ev} P_a P_b \sum_{y=0}^{a-1} \{C(t,a,y) - n_{g,eq}\}\{C(t,a,y+1) - n_{g,eq}\} \right]^{-1}, \tag{22}$$

the interface can not be kept atomically flat. Thus the second criterion determines the maximum size $L'_{\max}{}^{(2)}$ in the reduced unit from

$$\mathbf{C2}: \int_0^{L'^{(2)}_{\max}} \frac{dy}{u} \cdot \int_0^{L'^{(2)}_{\max}} u(y)u(y+1/l)dy = 4P_b \sim 4. \tag{23}$$

The first criterion **C1** represents that the low-density central portion will be left behind from the growth, whereas the second criterion **C2** represents that the growth originating from various positions on an edge leads to an uncorrelated interface. From **C1** or **C2**, one can determine $L'_{\max}{}^{(1)}$ or $L'_{\max}{}^{(2)}$, which are independent of μ_s and T. In the physical unit, then, the maximum sizes of a square crystal $L_{\max}{}^{(1),(2)}$ are obtained as

$$L_{\max}^{(1),(2)} \cong L'^{(1),(2)}_{\max} \cdot \frac{1}{\sqrt{8}} \exp\left((\varepsilon - \Delta\mu)/2T\right), \tag{24}$$

and the growth rates at the maximum size $V_s^{(1),(2)}$ are given as

$$V_s^{(1),(2)} \cong \left.\frac{da'}{dt'}\right|_{a'=L'^{(1),(2)}_{\max}} \cdot 4\exp\left((\Delta\mu - \varepsilon)/2T\right). \tag{25}$$

Since the coefficients, $L'^{(1),(2)}_{\max}$ and $d'a/dt'$, depend on n_g, the n_g-dependence of $L_{\max}^{(1),(2)}$ and $V_s^{(1),(2)}$ can not be represented in a scaling form.

5.3 Method of numerical solution

We now solve the diffusion equation (7) with boundary conditions, Eqs. (11) and (12) numerically, and compare the n_g-, μ_s/T- and t-dependence of growth rate V, the stability limit L_{max} and the concentration field with the scaling behaviors. The algorithm to be used is an explicit finite difference scheme (19). The space is divided into small grids, even though the crystal interface at $(x, a(t))$ or $(a(t), y)$ is not restricted on the grid points. On an i-th grid point outside of the crystal, a continuous value of a diffusion field $C_i(t)$ is assigned. The growth rate $\dot{a}(t)$ is calculated from the concentration field on the boundary grid points using Eq. (11). Then, we get the new interface position $a(t + \Delta t)$. Now, by solving the diffusion equation, we obtain new values of the diffusion field $C_i(t + \Delta t)$ except on the boundary points just contiguous to the crystal. The values of $C_i(t + \Delta t)$ on the boundary are obtained from the continuity condition Eq. (12) as $C_i(t + \Delta t) = C_{i+\delta}(t + \Delta t) - \dot{a}(t)\cdot\delta$. Here $(i + \delta)$-th site is the nearest position to the i-th site and belongs to the interior of the gas phase. These procedures complete the renewal of the diffusion field at a time $t + \Delta t$. Returning to the calculation of the velocity $\dot{a}(t + \Delta t)$, we can continue the iteration. The stability criterion **C1** and **C2** are judged in the iteration.

An initial condition is chosen to be the same with the Monte Carlo simulation, while outer boundary condition (i.e. $C(R = \infty) = n_g$) is improved such that the particle reservoir (i.e. the region with constant gas density n_g) is shifted outwardly when the density at some point in front of this region is depressed less than 99.5% of the prescribed value, n_g.

5.4 Results of numerical solution

For a fixed gas density, $n_g = 0.5$, the concentration field at various chemical potentials μ_s is found to be scaled as $C(\boldsymbol{r}; \mu_s) = \tilde{C}(\boldsymbol{r}/L_{max}^{(1)})$ (see Fig. 6). The maximum size $L_{max}^{(1)}$ determined with the criterion **C1** is found to be proportional to $\exp((\varepsilon - \Delta\mu)/2T)$, as is expected in Eq. (24) and is plotted in Fig. 5a. Here $\ln(L_{max}^{(2)})$ determined with the criterion **C2** and $\ln(L_{max})$ of the Monte Carlo simulation are also plotted. The L_{max}'s derived from Monte Carlo simulation lie between $L_{max}^{(1)}$ and $L_{max}^{(2)}$, the former being always larger than the latter.

If we fix a chemical potential $\mu_s = 10$, but vary n_g from 0.2 to 1.0, we observe a complicated variation of concentration field, especially in its orientation dependence (Fig. 7). The concentration field looks isotropic at low n_g, while at a high n_g (≥ 0.6) concentration field become anisotropic and lies parallel to the interface as is shown in Fig. 7. Therefore, we cannot expect a scaling behavior in a concentration field as a function of the gas density. The dependence of $L_{max}^{(1)}$ and $L_{max}^{(2)}$ on the gas density n_g is shown in Fig. 5b. Here also L_{max} lies between $L_{max}^{(1)}$ and $L_{max}^{(2)}$ One thing to be noted is that $L_{max}^{(1)}$ increase drastically as n_g approaches unity. The reason of this peculiar behavior may be that since there are plenty of gas atoms, the density at the center of the edge can not easily vanish any more. In these situations **C2** may

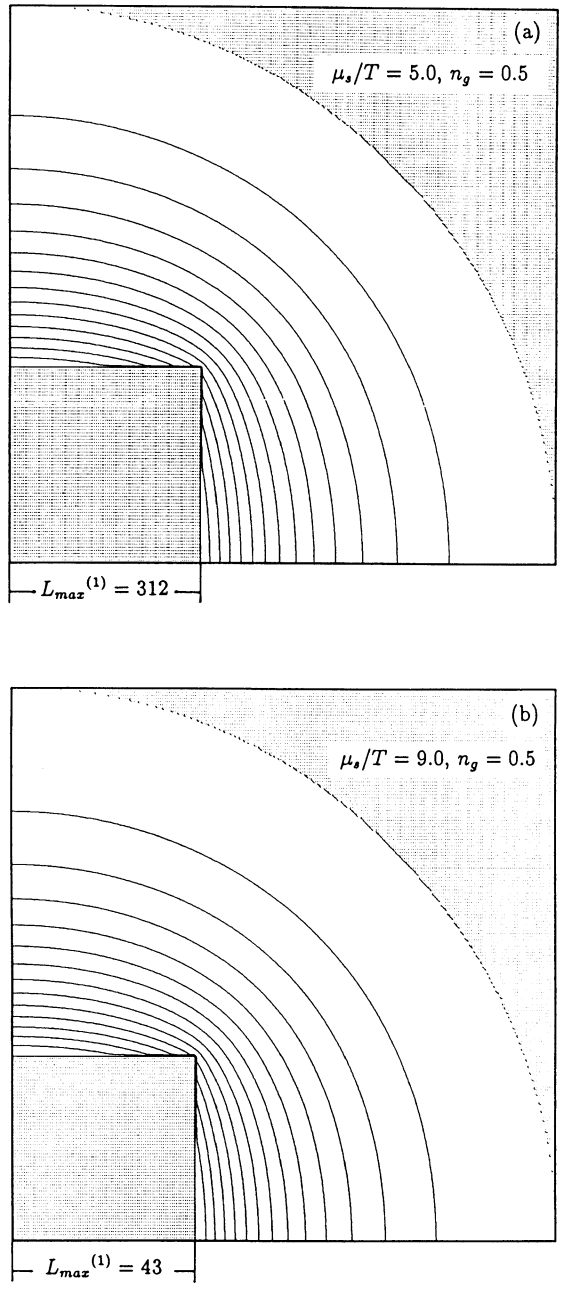

Fig. 6. Contours of constant gas density around the square crystal at the stability limit decided by criterion **C1**, with $n_g = 0.5$ and at (a) $\mu_s/T = 5.0$, and at (b) $\mu_s/T = 9.0$.

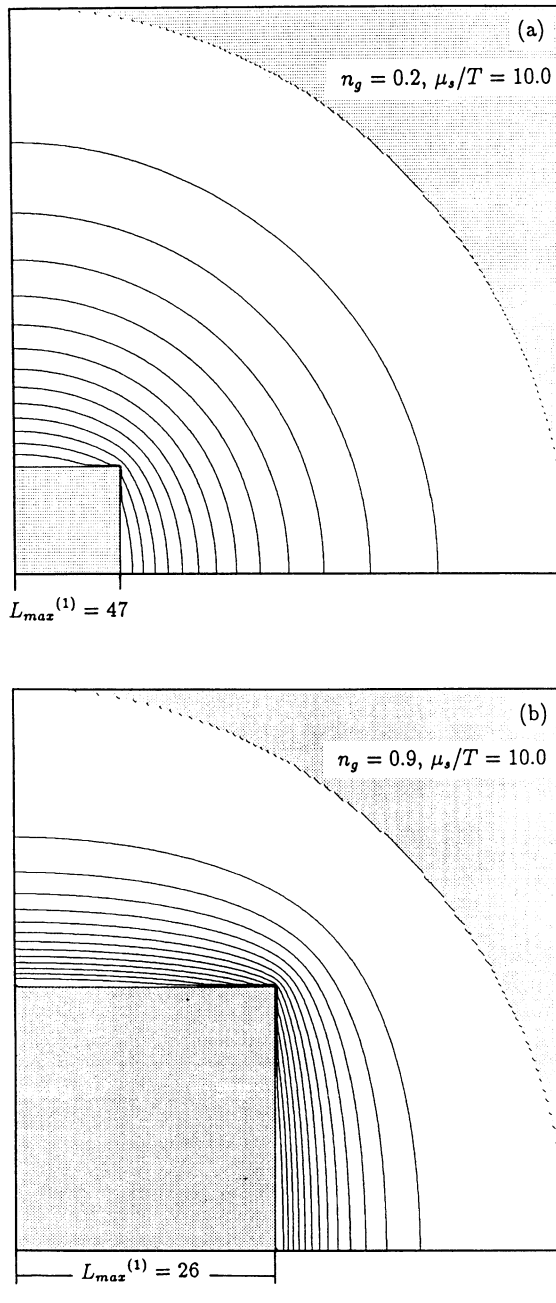

Fig. 7. Contours of constant gas density around the square crystal at the stability limit decided by criterion **C1** at $\mu_s/T = 10.0$ and with (a) $n_g = 0.2$ and with (b) $n_g = 0.9$.

be a better criterion for determining the stability limit.

We now investigate the time evolution of the crystal size. For a fixed gas density $n_g = 0.5$, the time evolution of the scaled crystal size a' at various chemical potential, μ_s, is plotted as a function of the scaled time t' in Fig. 8. Except the initial transient, one observes the universal scaling for $\mu_s/T \leq 10.0$. Even though a is not proportional to the time, the diagonal length $\sqrt{2}\,a(t)$ agrees with early part of the tip separation $r_{tip}(t)$ obtained by the Monte Carlo simulation (Fig. 9a). After the shape instability, the crystal turns into dendritic form but the tip grows steadily with the same velocity at the stability limit. The concentration field around the tip thus should remain the same with that of the square crystal at the stability limit. For n_g higher than 0.6, $a(t)$ deviates significantly from $r_{tip}(t)$ (Fig. 9b). This may indicate that the crystal growth at $n_g \geq 0.6$ is no longer controlled by surface kinetics.

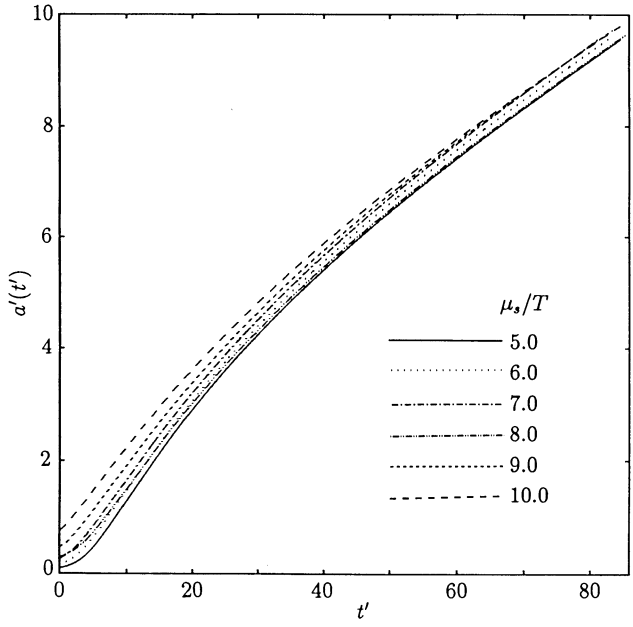

Fig. 8. Time evolution of the scaled crystal size $a'(t')$ for various μ_s/T at $n_g = 0.5$ and $T/J = 0.3$.

The $(\varepsilon - \mu_s)/T$ dependence of V and $V_s^{(1)} = \sqrt{2}\dot{a}$ at the stability limit, $a = L_{max}^{(1)}$, is shown in Fig. 3a. Here the growth rate $V_s^{(2)} = \sqrt{2}\dot{a}$ at $a = L_{max}^{(2)}$ is also plotted for comparison. Both $V_s^{(1)}$ and $V_s^{(2)}$ satisfy the relation Eq. (25). From this figure one clearly finds that V agrees $V_s^{(1)}$ for $(\varepsilon - \mu_s)/T \leq 6$. For $(\varepsilon - \mu_s)/T > 6$, the simulation

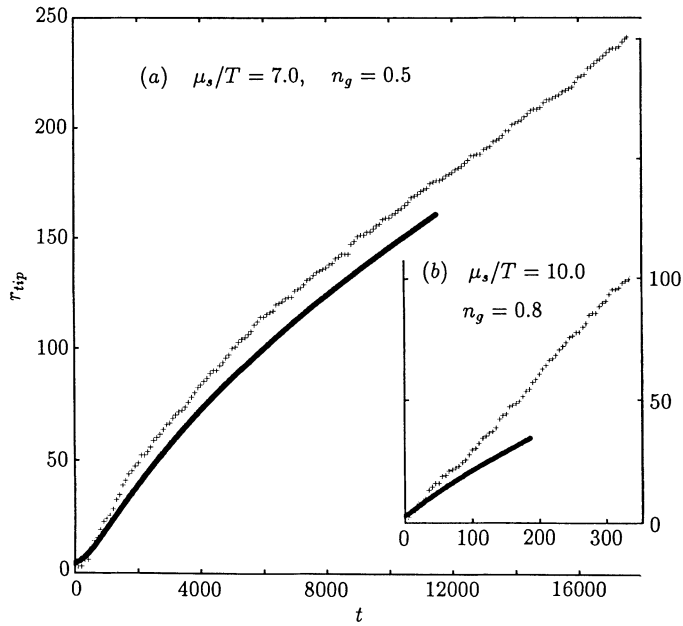

Fig. 9. Comparison of the time evolution of a tip separation r_{tip} of the crystal from the origin obtained by the Monte Carlo simulation (plotted by symbol +) and from the single nucleation theory (a thick solid line) at (a) $\mu_s/T = 7.0$ and $n_g = 0.5$, and at (b) $\mu_s/T = 10.0$ and $n_g = 0.8$.

data with the boundary condition **B.C.2** lie higher than $V_s^{(1)}$. This point will be discussed in the next section. The dependence of $V_s^{(1)}$, $V_s^{(2)}$ and V on gas density, n_g, is plotted in Fig. 3b. At a low density $n_g \leq 0.5$, V and $V_s^{(1)}$ show good agreement, while for n_g higher than 0.6, V deviates from $V_s^{(1)}$ and also from $V_s^{(2)}$ rapidly. The latter behavior is compatible with the previous $a(t)$-$r_{tip}(t)$ relation, indicating that the surface kinetics looses the control of the crystal growth.

6. Summary and Discussions

Crystal shapes are simulated by using a lattice gas model, which incorporates the surface tension and surface kinetics, chemical potentials of the solid, and also the diffusion dynamics in the gas phase. For a closed system at various temperatures, equilibrium shapes obtained on a square lattice agree with the exact profiles of the corresponding Ising model. Crystal sizes also agree with the values obtained by minimizing the free energy. For an open system with a particle reservoir of a fixed gas density, various growth shapes are obtained. On decreasing the energy cost ($\varepsilon - \mu_s$) in nucleating an isolated solid atom on a flat edge, growth shapes

changes from a polygonal, to a hopper and then to a dendritic and to a fractal, and finally to a compact structure, consecutively. Such variation is observed in a 3-dimensional experiment of cyclohexanol crystal growth from a pure melt (20). Crystal growth at large $(\varepsilon - \mu_s)/T$ is characterized by the exponential dependence of the maximum size of the polygonal crystal L_{max} as $L_{max} \sim \exp((\varepsilon - \Delta\mu)/2T)$, where $\Delta\mu$ is the chemical potential difference between the solid and the gas phase. The $(\varepsilon - \mu_s)/T$ dependence of growth rate V is inverse to that of L_{max}.

In the simulation, we have obtained the $(\varepsilon - \mu_s)/T$-dependence of V as $V \sim \exp(-0.29(\varepsilon - \mu_s)/T)$ (15). This dependence is obtained by fitting the velocity data at $11 \geq \mu_s/T \geq 4$. For $11 \geq \mu_s/T \geq 8$, simulation data of V agree with the numerical solution $V_s^{(1)}$ of the diffusion equation, whereas for $\mu_s/T \leq 7$, V lies distinctly higher than $V_s^{(1)}$ (Fig. 3a). The data for $\mu_s/T \leq 7$, however, are found to be influenced strongly by the boundary condition **B.C.2**. Namely, if we use the boundary condition **B.C.2** in the numerical solution of diffusion equation (7), then the growth rate $V_s^{(1)}$ increases and agrees with the simulation result, V. Thus, in the Monte Carlo simulation application of the boundary condition **B.C.2** might had lead too strong a boundary effect on the growing tip. Our conclusion now is that the true dependence of V on the chemical potential μ_s is represented by Eq. (25) instead of the previous conclusion, Eq. (4).

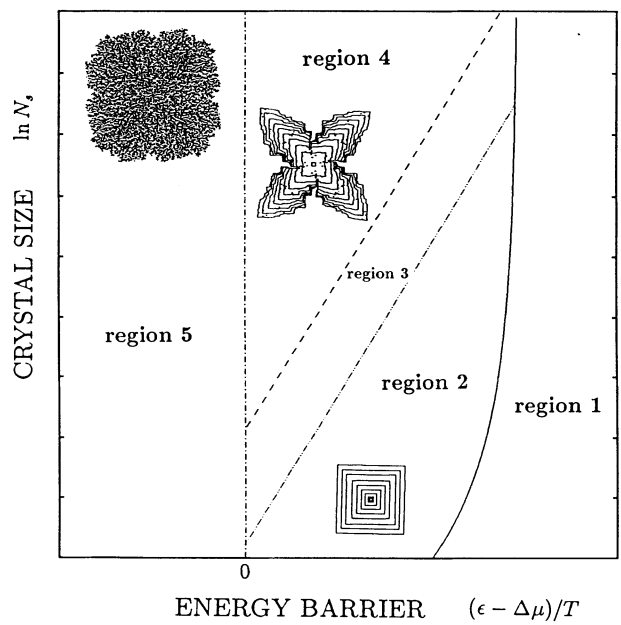

Fig. 10. Growth morphology of a crystal as a function of the crystal size, N_s, and the energy cost $(\varepsilon - \Delta\mu)/T$ to form a single atom nuclei on a flat surface at constant gas density. For detailed explanations see the main text.

We have introduced two criteria to decide the stability limit of the square crystal. The criterion **C1** is $C(L_{max}, 0)$ or $C(0, L_{max}) = n_{g,eq}$, and the criterion **C2** represents the effect of kinetic roughening. Both **C1** and **C2** are compatible to the data of L_{max} as for the exponential dependence on $\varepsilon - \Delta\mu$. As for the absolute value of the growth rate in hopper or dendritic shape, Monte Carlo data agree better with the growth rate determined with **C1**. The morphology of the hopper-like crystal after the instability is also compatible to the stability mechanism of **C1**, that the center of the edge stops growing due to the density depression.

Our result may be summarized in the phase diagram, Fig. 10, in the parameter space of the energy barrier, $\varepsilon - \Delta\mu$, and the number of crystal atoms, N_s. In the **region 1** a nuclei can not grow but evaporates. In the **region 2** the crystal grows, keeping a polygonal shape. The **region 3** is the transition region from a polygonal to a hopper-like shape. In **region 4** a crystal takes a dendritic form. In **region 5** the crystal grows without energy barrier. The growth is limited by the gas diffusion, and the crystal acquires a dendritic, a fractal or a compact structure, depending on the gas density, n_g, and on the length scale (17). **Region 1** is bounded to the left by Eq. (3), and **region 5** by $\varepsilon = \Delta\mu$ to the right. **Region 3** is bounded from **region 2** by $L_{max}^{(2)}$ given by Eq. (24), and from **region 4** by $L_{max}^{(1)}$.

REFERENCES

(1) Langer, J. S. (1980), Rev. Mod. Phys., **B52**, 1.
(2) Yokoyama, E. and Kuroda, T. (1990), Phys. Rev., **A41**, 2038.
(3) Trivedi, R. (1984), Metal. Trans., **B15A**, 977.
(4) Huang, S. C. and Glicksman, M. E. (1981), Acta Metall., **B29**, 701, and ibid, **B29**, 717.
(5) Witten, T. A. and Sander, L. M. (1981), Phys. Rev. Lett., **47**, 1400.
(6) Witten, T. A. and Sander, L. M. (1983), Phys. Rev., **B27**, 5686.
(7) Karma, A. (1986), Phys. Rev. Lett., **57**, 858.
(8) Karma, A. (1986), Phys. Rev., **B34**, 4353.
(9) Dombre, T. and Hakim, V. (1987), Phys. Rev., **A36**, 2811.
(10) Ben Amar, M. and Moussallam, B. (1988), Phys. Rev. Lett., **60**, 317.
(11) Saito, Y., Misbah, C., and Müller-Krumbhaar, H. (1989), Phys. Rev. Lett., **63**, 2377.
(12) Rottman, C. and Wortis, M. (1984), Phys. Rev., **B29**, 328.
(13) Akutsu, Y. and Akutsu, N. (1987), J. Phys. Soc. Jpn., **56**, 9.
(14) Rottman, C. and Wortis, M. (1981), Phys. Rev., **B24**, 6274.
(15) Saito, Y. and Ueta, T. (1989), Phys. Rev., **A40**, 3408.
(16) Wulff, G., Kristallogr, Z. (1901), Miner., **34**, 449.
(17) Uwaha, M. and Saito, Y. (1989), Phys. Rev., **A40**, 4716.
(18) Chernov, A. A. (1974), J. Crystal Growth, **24/25**, 11.
(19) Wilcox, W. R. (1977), J. Crystal Growth, **37**, 229.
(20) Ovsienko, R. E., Alfintsev, A., and Maslow, V. V., (1974), J. Crystal Growth, **26**, 233.